



# ASTRO-H Space X-ray Observatory White Paper

## Low-mass X-ray Binaries

C. Done (Durham University), M. Tsujimoto (JAXA), E. Cackett (University of Cambridge<sup>1</sup>),  
J. W. den Herder (SRON), T. Dotani (JAXA), T. Enoto (RIKEN), C. Ferrigno (Université de Genève),  
T. Kallman (NASA/GSFC), T. Kohmura (Tokyo University of Science), P. Laurent (CEA Saclay),  
J. Miller (University of Michigan), S. Mineshige (Kyoto University), H. Mori (Nagoya University),  
K. Nakazawa (University of Tokyo), F. Paerels (Columbia University), S. Sakurai (University of Tokyo),  
Y. Soong (NASA/GSFC), S. Sugita (Nagoya University), H. Takahashi (Hiroshima University),  
T. Tamagawa (RIKEN), Y. Tanaka (MPE), Y. Terada (Saitama University), and  
S. Uno (Nihon Fukushi University)  
on behalf of the ASTRO-H Science Working Group

### Abstract

There is still 10-20% uncertainty on the neutron star (NS) mass-radius relation. These uncertainties could be reduced by an order of magnitude through an unambiguous measure of  $M/R$  from the surface redshift of a narrow line, greatly constraining the Equation of State for ultra-dense material. It is possible that the SXS on *ASTRO-H* can detect this from an accreting neutron star with low surface velocity in the line of sight i.e. either low inclination or low spin. Currently there is only one known low inclination LMXB, Ser X-1, and one known slow spin LMXB, J17480-2446 in Terzan 5. Ser X-1 is a persistent source which is always in the soft state (banana branch), where the accreting material should form an equatorial belt around the neutron star. A pole-on view should then allow the NS surface to be seen directly. A 100 ks observation should allow us to measure  $M/R$  if there are any heavy elements in the photosphere at the poles. Conversely, J17480-2446 in Terzan 5 is a transient accretion powered millisecond pulsar, where the accreting material is collimated onto the magnetic pole in the hard (island) state ( $L_x < 0.1L_{Edd}$ ). The hotspot where the shock illuminates the NS surface is clearly seen in this state. A 100 ks ToO observation of this (or any other similarly slow spin system) in this state, may again allow the surface redshift to be directly measured.

NS LMXB can also show winds from the outer disk, detected as H and He-like iron  $K\alpha$  absorption lines. The most likely origin of these winds is from thermal driving (helped by radiation pressure when  $L \sim L_{Edd}$ ). This makes clear predictions about the launch radius, acceleration, and mass loss rate in the wind. Each of these can be constrained with a 50 – 100 ks observation of the wind in the persistent source GX13+1. The ratio of emission to absorption (P Cygni profile) gives the solid angle of the wind, required to determine mass loss rates, while resolving the velocity width of the absorption gives much better constraints on the launch radius than derived from CCD data, and the detailed profile of the blue wing of the absorption traces the acceleration. This will critically test the thermal wind model of the disk wind.

---

<sup>1</sup>Present address: Wayne University

## Complete list of the ASTRO-H Science Working Group

Tadayuki Takahashi<sup>a</sup>, Kazuhisa Mitsuda<sup>a</sup>, Richard Kelley<sup>b</sup>, Felix Aharonian<sup>c</sup>, Hiroki Akamatsu<sup>d</sup>, Fumie Akimoto<sup>e</sup>, Steve Allen<sup>f</sup>, Naohisa Anabuki<sup>g</sup>, Lorella Angelini<sup>b</sup>, Keith Arnaud<sup>b</sup>, Marc Audard<sup>i</sup>, Hisamitsu Awaki<sup>j</sup>, Aya Bamba<sup>k</sup>, Marshall Bautz<sup>l</sup>, Roger Blandford<sup>f</sup>, Laura Brenneman<sup>b</sup>, Greg Brown<sup>m</sup>, Edward Cackett<sup>n</sup>, Maria Chernyakova<sup>c</sup>, Meng Chiao<sup>b</sup>, Paolo Coppi<sup>o</sup>, Elisa Costantini<sup>d</sup>, Jelle de Plaa<sup>d</sup>, Jan-Willem den Herder<sup>d</sup>, Chris Done<sup>p</sup>, Tadayasu Dotani<sup>a</sup>, Ken Ebisawa<sup>a</sup>, Megan Eckart<sup>b</sup>, Teruaki Enoto<sup>q</sup>, Yuichiro Ezoe<sup>r</sup>, Andrew Fabian<sup>n</sup>, Carlo Ferrigno<sup>i</sup>, Adam Foster<sup>s</sup>, Ryuichi Fujimoto<sup>l</sup>, Yasushi Fukazawa<sup>u</sup>, Stefan Funk<sup>f</sup>, Akihiro Furuzawa<sup>e</sup>, Massimiliano Galeazzi<sup>v</sup>, Luigi Gallo<sup>w</sup>, Poshak Gandhi<sup>p</sup>, Matteo Guainazzi<sup>x</sup>, Yoshito Haba<sup>y</sup>, Kenji Hamaguchi<sup>h</sup>, Isamu Hatsukade<sup>z</sup>, Takayuki Hayashi<sup>a</sup>, Katsuhiro Hayashi<sup>a</sup>, Kiyoshi Hayashida<sup>g</sup>, Junko Hiraga<sup>aa</sup>, Ann Hornschemeier<sup>b</sup>, Akio Hoshino<sup>ab</sup>, John Hughes<sup>ac</sup>, Una Hwang<sup>ad</sup>, Ryo Iizuka<sup>a</sup>, Yoshiyuki Inoue<sup>a</sup>, Hajime Inoue<sup>a</sup>, Kazunori Ishibashi<sup>e</sup>, Manabu Ishida<sup>a</sup>, Kumi Ishikawa<sup>q</sup>, Yoshitaka Ishisaki<sup>f</sup>, Masayuki Ito<sup>ae</sup>, Naoko Iyomoto<sup>af</sup>, Jelle Kaastra<sup>d</sup>, Timothy Kallman<sup>b</sup>, Tuneyoshi Kamae<sup>f</sup>, Jun Kataoka<sup>ag</sup>, Satoru Katsuda<sup>a</sup>, Junichiro Katsuta<sup>u</sup>, Madoka Kawaharada<sup>a</sup>, Nobuyuki Kawai<sup>ah</sup>, Dmitry Khangulyan<sup>a</sup>, Caroline Kilbourne<sup>b</sup>, Masashi Kimura<sup>ai</sup>, Shunji Kitamoto<sup>ab</sup>, Tetsu Kitayama<sup>aj</sup>, Takayoshi Kohmura<sup>ak</sup>, Motohide Kokubun<sup>a</sup>, Saori Konami<sup>r</sup>, Katsuji Koyama<sup>al</sup>, Hans Krimm<sup>b</sup>, Aya Kubota<sup>am</sup>, Hideyo Kunieda<sup>e</sup>, Stephanie LaMassa<sup>o</sup>, Philippe Laurent<sup>an</sup>, François Lebrun<sup>an</sup>, Maurice Leutenegger<sup>b</sup>, Olivier Limousin<sup>an</sup>, Michael Loewenstein<sup>b</sup>, Knox Long<sup>ao</sup>, David Lumb<sup>ap</sup>, Grzegorz Madejski<sup>f</sup>, Yoshitomo Maeda<sup>a</sup>, Kazuo Makishima<sup>aa</sup>, Maxim Markevitch<sup>b</sup>, Hironori Matsumoto<sup>e</sup>, Kyoko Matsushita<sup>aq</sup>, Dan McCammon<sup>ar</sup>, Brian McNamara<sup>as</sup>, Jon Miller<sup>at</sup>, Eric Miller<sup>l</sup>, Shin Mineshige<sup>au</sup>, Ikuyuki Mitsuishi<sup>e</sup>, Takuya Miyazawa<sup>e</sup>, Tsunefumi Mizuno<sup>u</sup>, Koji Mori<sup>z</sup>, Hideyuki Mori<sup>e</sup>, Koji Mukai<sup>b</sup>, Hiroshi Murakami<sup>av</sup>, Toshio Murakami<sup>t</sup>, Richard Mushotzky<sup>h</sup>, Ryo Nagino<sup>g</sup>, Takao Nakagawa<sup>a</sup>, Hiroshi Nakajima<sup>g</sup>, Takeshi Nakamori<sup>aw</sup>, Shinya Nakashima<sup>a</sup>, Kazuhiro Nakazawa<sup>aa</sup>, Masayoshi Nobukawa<sup>al</sup>, Hirofumi Noda<sup>q</sup>, Masaharu Nomachi<sup>ax</sup>, Steve O' Dell<sup>ay</sup>, Hirokazu Odaka<sup>a</sup>, Takaya Ohashi<sup>r</sup>, Masanori Ohno<sup>u</sup>, Takashi Okajima<sup>b</sup>, Naomi Ota<sup>az</sup>, Masanobu Ozaki<sup>a</sup>, Frits Paerels<sup>ba</sup>, Stéphane Paltani<sup>i</sup>, Arvind Parmar<sup>x</sup>, Robert Petre<sup>b</sup>, Ciro Pinto<sup>n</sup>, Martin Pohl<sup>i</sup>, F. Scott Porter<sup>b</sup>, Katja Pottschmidt<sup>b</sup>, Brian Ramsey<sup>ay</sup>, Rubens Reis<sup>at</sup>, Christopher Reynolds<sup>h</sup>, Claudio Ricci<sup>au</sup>, Helen Russell<sup>n</sup>, Samar Safi-Harb<sup>bb</sup>, Shinya Saito<sup>a</sup>, Hiroaki Sameshima<sup>a</sup>, Goro Sato<sup>ag</sup>, Kosuke Sato<sup>aq</sup>, Rie Sato<sup>a</sup>, Makoto Sawada<sup>k</sup>, Peter Serlemitsos<sup>b</sup>, Hiromi Seta<sup>bc</sup>, Aurora Simionescu<sup>a</sup>, Randall Smith<sup>s</sup>, Yang Soong<sup>b</sup>, Łukasz Stawarz<sup>a</sup>, Yasuharu Sugawara<sup>bd</sup>, Satoshi Sugita<sup>j</sup>, Andrew Szymkowiak<sup>o</sup>, Hiroyasu Tajima<sup>e</sup>, Hiromitsu Takahashi<sup>u</sup>, Hiroaki Takahashi<sup>g</sup>, Yoh Takei<sup>a</sup>, Toru Tamagawa<sup>q</sup>, Takayuki Tamura<sup>a</sup>, Keisuke Tamura<sup>e</sup>, Takaaki Tanaka<sup>al</sup>, Yasuo Tanaka<sup>a</sup>, Yasuyuki Tanaka<sup>u</sup>, Makoto Tashiro<sup>bc</sup>, Yuzuru Tawara<sup>e</sup>, Yukikatsu Terada<sup>bc</sup>, Yuichi Terashima<sup>j</sup>, Francesco Tombesi<sup>b</sup>, Hiroshi Tomida<sup>ai</sup>, Yohko Tsuboi<sup>bd</sup>, Masahiro Tsujimoto<sup>a</sup>, Hiroshi Tsunemi<sup>g</sup>, Takeshi Tsuru<sup>al</sup>, Hiroyuki Uchida<sup>al</sup>, Yasunobu Uchiyama<sup>ab</sup>, Hideki Uchiyama<sup>be</sup>, Yoshihiro Ueda<sup>au</sup>, Shutaro Ueda<sup>g</sup>, Shiro Ueno<sup>ai</sup>, Shinichiro Uno<sup>bf</sup>, Meg Urry<sup>o</sup>, Eugenio Ursino<sup>v</sup>, Cor de Vries<sup>d</sup>, Shin Watanabe<sup>a</sup>, Norbert Werner<sup>f</sup>, Dan Wilkins<sup>w</sup>, Shinya Yamada<sup>r</sup>, Hiroya Yamaguchi<sup>b</sup>, Kazutaka Yamaoka<sup>e</sup>, Noriko Yamasaki<sup>a</sup>, Makoto Yamauchi<sup>z</sup>, Shigeo Yamauchi<sup>az</sup>, Tahir Yaqoob<sup>b</sup>, Yoichi Yatsu<sup>ah</sup>, Daisuke Yonetoku<sup>t</sup>, Atsumasa Yoshida<sup>k</sup>, Takayuki Yuasa<sup>q</sup>, Irina Zhuravleva<sup>f</sup>, Abderahmen Zoghbi<sup>h</sup>, and John ZuHone<sup>b</sup>

<sup>a</sup>Institute of Space and Astronautical Science (ISAS), Japan Aerospace Exploration Agency (JAXA), Kanagawa 252-5210, Japan

<sup>b</sup>NASA/Goddard Space Flight Center, MD 20771, USA

<sup>c</sup>Astronomy and Astrophysics Section, Dublin Institute for Advanced Studies, Dublin 2, Ireland

<sup>d</sup>SRON Netherlands Institute for Space Research, Utrecht, The Netherlands

<sup>e</sup>Department of Physics, Nagoya University, Aichi 338-8570, Japan

<sup>f</sup>Kavli Institute for Particle Astrophysics and Cosmology, Stanford University, CA 94305, USA

<sup>g</sup>Department of Earth and Space Science, Osaka University, Osaka 560-0043, Japan

<sup>h</sup>Department of Astronomy, University of Maryland, MD 20742, USA

<sup>i</sup>Université de Genève, Genève 4, Switzerland

<sup>j</sup>Department of Physics, Ehime University, Ehime 790-8577, Japan

<sup>k</sup>Department of Physics and Mathematics, Aoyama Gakuin University, Kanagawa 229-8558, Japan

<sup>l</sup>Kavli Institute for Astrophysics and Space Research, Massachusetts Institute of Technology, MA 02139, USA

<sup>m</sup>Lawrence Livermore National Laboratory, CA 94550, USA

<sup>n</sup>Institute of Astronomy, Cambridge University, CB3 0HA, UK

<sup>o</sup>Yale Center for Astronomy and Astrophysics, Yale University, CT 06520-8121, USA

<sup>p</sup>Department of Physics, University of Durham, DH1 3LE, UK

<sup>q</sup>RIKEN, Saitama 351-0198, Japan

<sup>r</sup>Department of Physics, Tokyo Metropolitan University, Tokyo 192-0397, Japan

<sup>s</sup>Harvard-Smithsonian Center for Astrophysics, MA 02138, USA

- <sup>t</sup>Faculty of Mathematics and Physics, Kanazawa University, Ishikawa 920-1192, Japan
- <sup>u</sup>Department of Physical Science, Hiroshima University, Hiroshima 739-8526, Japan
- <sup>v</sup>Physics Department, University of Miami, FL 33124, USA
- <sup>w</sup>Department of Astronomy and Physics, Saint Mary's University, Nova Scotia B3H 3C3, Canada
- <sup>x</sup>European Space Agency (ESA), European Space Astronomy Centre (ESAC), Madrid, Spain
- <sup>y</sup>Department of Physics and Astronomy, Aichi University of Education, Aichi 448-8543, Japan
- <sup>z</sup>Department of Applied Physics, University of Miyazaki, Miyazaki 889-2192, Japan
- <sup>aa</sup>Department of Physics, University of Tokyo, Tokyo 113-0033, Japan
- <sup>ab</sup>Department of Physics, Rikkyo University, Tokyo 171-8501, Japan
- <sup>ac</sup>Department of Physics and Astronomy, Rutgers University, NJ 08854-8019, USA
- <sup>ad</sup>Department of Physics and Astronomy, Johns Hopkins University, MD 21218, USA
- <sup>ae</sup>Faculty of Human Development, Kobe University, Hyogo 657-8501, Japan
- <sup>af</sup>Kyushu University, Fukuoka 819-0395, Japan
- <sup>ag</sup>Research Institute for Science and Engineering, Waseda University, Tokyo 169-8555, Japan
- <sup>ah</sup>Department of Physics, Tokyo Institute of Technology, Tokyo 152-8551, Japan
- <sup>ai</sup>Tsukuba Space Center (TKSC), Japan Aerospace Exploration Agency (JAXA), Ibaraki 305-8505, Japan
- <sup>aj</sup>Department of Physics, Toho University, Chiba 274-8510, Japan
- <sup>ak</sup>Department of Physics, Tokyo University of Science, Chiba 278-8510, Japan
- <sup>al</sup>Department of Physics, Kyoto University, Kyoto 606-8502, Japan
- <sup>am</sup>Department of Electronic Information Systems, Shibaura Institute of Technology, Saitama 337-8570, Japan
- <sup>an</sup>IRFU/Service d'Astrophysique, CEA Saclay, 91191 Gif-sur-Yvette Cedex, France
- <sup>ao</sup>Space Telescope Science Institute, MD 21218, USA
- <sup>ap</sup>European Space Agency (ESA), European Space Research and Technology Centre (ESTEC), 2200 AG Noordwijk, The Netherlands
- <sup>aq</sup>Department of Physics, Tokyo University of Science, Tokyo 162-8601, Japan
- <sup>ar</sup>Department of Physics, University of Wisconsin, WI 53706, USA
- <sup>as</sup>University of Waterloo, Ontario N2L 3G1, Canada
- <sup>at</sup>Department of Astronomy, University of Michigan, MI 48109, USA
- <sup>au</sup>Department of Astronomy, Kyoto University, Kyoto 606-8502, Japan
- <sup>av</sup>Department of Information Science, Faculty of Liberal Arts, Tohoku Gakuin University, Miyagi 981-3193, Japan
- <sup>aw</sup>Department of Physics, Faculty of Science, Yamagata University, Yamagata 990-8560, Japan
- <sup>ax</sup>Laboratory of Nuclear Studies, Osaka University, Osaka 560-0043, Japan
- <sup>ay</sup>NASA/Marshall Space Flight Center, AL 35812, USA
- <sup>az</sup>Department of Physics, Faculty of Science, Nara Women's University, Nara 630-8506, Japan
- <sup>ba</sup>Department of Astronomy, Columbia University, NY 10027, USA
- <sup>bb</sup>Department of Physics and Astronomy, University of Manitoba, MB R3T 2N2, Canada
- <sup>bc</sup>Department of Physics, Saitama University, Saitama 338-8570, Japan
- <sup>bd</sup>Department of Physics, Chuo University, Tokyo 112-8551, Japan
- <sup>be</sup>Science Education, Faculty of Education, Shizuoka University, Shizuoka 422-8529, Japan
- <sup>bf</sup>Faculty of Social and Information Sciences, Nihon Fukushi University, Aichi 475-0012, Japan

# Contents

<b>1</b>	<b>Introduction</b>	<b>5</b>
<b>2</b>	<b>The Equation of State for Nuclear Matter</b>	<b>6</b>
2.1	Background and Previous Studies . . . . .	6
2.2	Prospects & Strategy . . . . .	6
2.3	Targets & Feasibility . . . . .	8
2.3.1	Low inclination . . . . .	8
2.3.2	Beyond Feasibility: low inclination . . . . .	9
2.3.3	Slow spin . . . . .	9
2.3.4	Beyond Feasibility: slow spin . . . . .	10
2.3.5	Phase resolved emission . . . . .	11
<b>3</b>	<b>Linking outflows to inflows in strong gravity: Winds in absorption</b>	<b>11</b>
3.1	Background and Previous Studies . . . . .	11
3.2	Prospects & Strategy . . . . .	11
3.3	Targets & Feasibility . . . . .	12
3.4	Beyond Feasibility . . . . .	13
<b>4</b>	<b>Linking outflows to inflows in strong gravity: Winds in emission</b>	<b>13</b>
4.1	Background and Previous Studies . . . . .	13
4.2	Prospects & Strategy . . . . .	14
4.3	Targets & Feasibility . . . . .	14
4.4	Beyond Feasibility . . . . .	14
<b>5</b>	<b>Spectral modelling requirements</b>	<b>14</b>
<b>6</b>	<b>Summary of Top Science</b>	<b>15</b>



# 1 Introduction

Low Mass X-ray Binaries (LMXB) were the first compact accretion powered sources to be discovered (Sco X-1), where a neutron star (NS) accretes via Roche Lobe overflow from a companion star. NS have similar  $M/R$  to the last stable orbit around a moderate spin black hole (BH), so their accretion flows should be similar. The difference is that the NS have a solid surface, while black holes do not. The surface means that there is the possibility of X-ray bursts from nuclear burning of the accreted material onto the surface, or coherent pulsations from magnetically collimated accretion as well as a boundary layer between the flow and the surface which produces both an additional emission component and an additional source of turbulence (high frequency noise). However, the most important possibility from the surface is that there could be atomic features. Their gravitational redshift would give a direct, accurate, measure of  $M/R$  to observationally constrain the quantum chromodynamics (via the equation of state) at densities which are far beyond those currently accessible to laboratory experiments.

Another difference between the NS and BH is that the NS has smaller mass. Thus a given type of companion star must be closer in order to overflow its Roche lobe. The disk is truncated by tidal forces at about half the orbital separation so the disk is smaller and hence less likely to dip below the Hydrogen ionisation temperature which causes the disk instability (King et al. 1996). Thus many NS are persistent sources, making targeting and scheduling easier than in the typically transient BH. Disk-jet coupling, the physics of the accretion flow, the origin of the quasi-periodic oscillations (both low and high frequencies), and the origin of winds from the disk are all issues which can be addressed using the NS systems as well as the BH. For example, disk accreting NS LMXB (atolls) show the same hard/soft spectral transition as seen in BH, going from the island state (hard) to banana branch (soft) to Z sources (Eddington and above) as the mass accretion rate increases (Lin, Remillard & Homan 2009).

The disk size is also important in determining whether the system should power an equatorial disk wind. X-ray illumination heats the upper layers of the disk to the Compton temperature. At small radii this is still bound, so forms a static ‘corona’ (a confusing name as this is unrelated to the intrinsic hard X-ray source which is also termed ‘coronal’). At larger radii, the velocity associated with the Compton temperature is sufficient for the material to escape as a thermally driven wind. Since NS typically have smaller disks than BH, winds should be rarer, seen only in the largest separation binary systems.

The vertical structure from the static ‘corona’ (and wind), together with the interaction of the accretion stream with the disk, gives an inclination dependence to LMXB spectra. At low inclinations there is an unobscured view of the inner disk, at higher inclinations there can be absorption lines from the ‘corona’ (and wind), at even higher inclinations there are also periodic absorption dips from the clumpy impact of the stream and disk (dippers), and at extreme inclinations, we see the central source only via scattering in the ‘corona’ as a direct view is obscured by the disk and/or companion star (Accretion Disk Corona: ADC sources e.g. Frank, King & Raine 1987).

However, the key property of the NS, that of its surface, gives rise to some distinctive behaviour. LMXB are old systems, and the NS surface field is low (below  $10^{10}$  G in order to show bursts). Measured fields are a few  $\times 10^8$  G from the handful of systems which show magnetically collimated accretion - the accretion powered millisecond X-ray pulsars (AMXP). Surface fields must be lower in the transient NS as these do not show pulses at similarly low mass accretion rates. This is generally explained by them having a higher long term average mass accretion rate which buries a similarly strong surface field (Cumming et al. 2001, but see Lamb et al. 2009 for an alternative).

Unlike the BH in LMXB (King & Kolb 1999), the spins of NS in LMXB have changed substantially during their lifetime. Firstly, they spin down from their birth via a rotation powered pulsar phase, then when the binary makes contact they spin up via the accretion of angular momentum as seen by the fast spins inferred from burst oscillations in LMXB (see e.g. the review by Patruno & Watts 2012). The accretion rate declines as the binary evolves, so the magnetic field can emerge from the surface and give an AMSP. Eventually the accretion rate becomes so low that the NS can re-emerge as a low field ( $\sim 10^8$  G) rotation powered millisecond pulsar, where the pulsar wind ablates the companion star, hastening its demise (black widow pulsars and red backs: Papitto

et al. 2013).

## 2 The Equation of State for Nuclear Matter

### 2.1 Background and Previous Studies

The mean density of a NS is  $2-3\times$ nuclear, and their central densities are much higher. This is a regime in which quantum chromodynamics cannot be tested in laboratory experiments, so there is considerable uncertainty in the equation of state (EoS) models. Current constraints from mass measurements of NS already favour a 'normal nucleon' EoS, giving predicted radii which do not depend much on mass from  $1-2M_{\odot}$  at  $11-12$  km ( $\sim 7-3.5R_g$  e.g. Özel 2013). However, there are still a range of models within this region, and substantial model uncertainties even for a given EoS (Hebeler et al. 2013). Better astrophysical data would give clear input to the nuclear physics community to constrain their models.

Constraints on  $M/R$  can be made in a variety of ways:

- a) redshift of any narrow lines emitted from the photosphere of the NS (SXS)
- b) redshift of the broad iron line from reflection from the accretion disk as the inner edge of the disk is an upper limit on the size of the NS (SXS to get detailed line shape without pileup and resolve out narrow emission/absorption features, plus broad band spectrum to constrain the complex continuum)
- c) detailed pulse profile modelling of accreting millisecond pulsars and burst oscillations (broad band spectra)
- d) a direct measure of the radius from the luminosity and temperature of thermal radiation from the NS surface cooling after accretion has stopped (broad band spectrum in quiescence)

The problem is important enough that all of these approaches need to be used as it is only when we get consistent answers from multiple methods that there can be real confidence in the result. Nonetheless, only measuring redshift from a narrow line offers the possibility of significantly improved constraints on  $M/R$  with *ASTRO-H*.

### 2.2 Prospects & Strategy

The SXS effective area around the iron K alpha line is almost an order of magnitude larger than the *Chandra* HETG, the only other high resolution instrument to cover this transition ( $225$  versus  $28$  cm<sup>2</sup> at  $6.5-7$  keV). However, this effective area gain in *ASTRO-H* is offset by the maximum count rate limit for pileup in bright sources, with the two instruments having equal usable counts at iron for a flux of  $\sim 4 \times 10^{-8}$  ergs cm<sup>2</sup> s<sup>-1</sup> for a soft transient with typical Galactic  $N_H \sim 6 \times 10^{21}$  cm<sup>2</sup>. Nonetheless, weak and *narrow* features are still more easily detected and characterised in *ASTRO-H* as its resolution is better by a factor  $\sim 8-10$  at iron, giving it significant discovery space even in bright sources.

To see narrow absorption lines from the NS surface requires that there are heavy elements in the photosphere, that these are not completely ionised, that the photosphere is not buried beneath the accretion flow, and that the resulting atomic features are not substantially broadened by thermal, magnetic or rotational effects.

Heavy elements are deposited onto the NS surface by the accretion flow. They are stopped by collisional processes, which are more efficient for higher mass/charge ions. Hence iron and other heavy elements are halted higher up in the photosphere than lower atomic number elements. They can then be destroyed by spallation bombardment (by the still energetic helium and hydrogen ions, transforming the iron nuclei to lower  $Z$  elements) or sink under gravity. The deposition and destruction rate both depend linearly on  $\dot{M}$  so the steady state Fe column is around solar, independent of  $\dot{M}$  for  $L_x > 6 \times 10^{32}$  ergs/s (Bildsten, Chang & Paerels 2003; Chang, Bildsten & Wasserman 2005). Thus there can be iron in the photosphere of an accreting NS, especially as the outwards radiation force on the line transitions act against gravity to keep iron (and other elements) from settling where these are not completely ionised (Chang, Bildsten & Wasserman 2005) i.e. for temperatures of less than  $\sim 1.5$  keV (Suleimanov, Poutanen & Werner 2012).

The surface can only be seen if it is not hidden beneath the accretion flow. This depends on the geometry of the accreting material as well as its optical depth. At low accretion rates, the accretion flow is hot and quasi-spherical interior to some truncation radius at which the thin disk evaporates (island state). There is additional

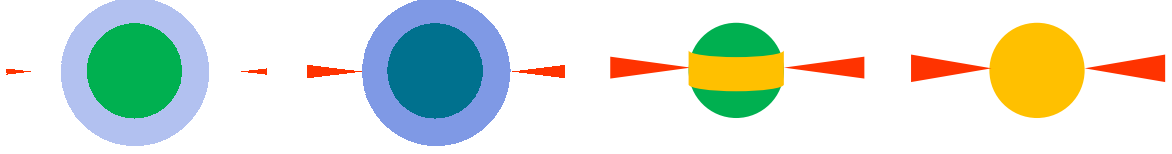


**Figure 1:** From left to right shows the changing geometry of the accretion flow onto the NS surface with  $L/L_{Edd}$  increasing from  $\sim 10^{-4}$ ,  $\sim 10^{-2}$ ,  $\sim 0.1$  and  $\sim 1$ . At the lowest mass accretion rates the disc (red) is truncated far from the NS surface (green), and the inner accretion flow/boundary layer is hot and optically thin (blue). The flow becomes more optically thick but remains hot as the mass accretion rate increases in the island state, so that the neutron star surface can still be seen through the translucent flow. The flow then collapses into a thin disc, so the boundary layer (yellow) forms an optically thick equatorial belt, which then extends upwards with increasing mass accretion rate to cover the entire surface.

luminosity from the boundary layer where this settles onto the surface, but the flow and boundary layer merge together, forming a single hot ( $\sim 30 - 50$  keV), optically thin(ish) ( $\tau \sim 1.5 - 2$ ) structure (Medvedev & Narayan 2001). A fraction  $e^{-\tau}$  of the surface emission should escape without scattering, so  $\sim 10 - 20\%$  of the intrinsic NS photosphere should be seen directly. The temperature of this surface emission can also be seen imprinted onto the low energy rollover of the Compton spectrum and is only  $\sim 0.5 - 0.6$  keV (e.g. Sakurai et al. 2012), so there should be atomic features (see Figure 1a and b).

At higher mass accretion rates ( $L \geq 0.1 - 0.5 L_{Edd}$ ), the thin disk extends down to the NS surface, forming a boundary layer where it impacts around the NS equator. The boundary layer is now optically thick ( $\tau \sim 5 - 10$ ) so hides the surface beneath it, though the temperature can still be seen via its imprint on the low energy rollover of the Compton spectrum at  $\sim 0.8 - 1.3$  keV. The boundary layer itself is at the local Eddington temperature of  $\sim 2.5$  keV (Revnivtsev, Suleimanov & Poutanen 2013), so is completely ionised. However, the vertical extent of the boundary layer depends on the accretion rate, and it only covers the entire surface, extending up the NS pole only when the accretion rate is around Eddington (Suleimanov & Poutanen 2006, Figure 1c and d).

Thus the surface is always at low enough temperatures to not be completely ionised, but is completely covered by the optically thick, completely ionised accretion flow at  $L \sim L_{Edd}$  (upper banana branch and Z sources). It is also completely covered by the much hotter (so still completely ionised) accretion flow at low mass accretion rates (island state), but here the material is not so optically thick so a fraction of the surface can be seen directly. Hence the largest fraction of surface emission would be seen from a pole-on view of a lower banana branch source, where the optically thick accretion flow is confined to an equatorial belt, or in an island state, where the accretion flow covers most of the surface but is optically thin(ish).

The surface can also be seen directly during X-ray bursts. Bursts have the advantage that there are almost certainly some heavy elements present in the photosphere due to dredge up in the thermonuclear explosion. However, the bursts reach high enough temperatures that all elements are completely ionised (Suleimanov et al. 2012). Bursts occur over only a small fraction of a total observation, and selecting only the cooler phases of the burst will limit the signal-to-noise even further, making this unlikely to be feasible.

Looking at the surface emission outside of the bursts may then be the better strategy. Any atomic features will be redshifted to  $E$  from  $E_0$  depending on the radius of the star  $r = R/R_g \propto R/M$  where  $r = 2/[1 - (E/E_0)^2]$  and  $E/E_0 \sim 0.8$  for typical NS parameters ( $r = 6$  corresponds to 12.6 km for  $1.4 M_\odot$  i.e. a surface redshift of 0.22, while a radius of 10 km gives a redshift of 0.30). This shift is the same over the entire surface for a spherical star, with thermal and Stark (pressure) broadening giving an intrinsic width of a few eV. Magnetic fields in the line-forming region broaden the lines via the Zeeman effect, giving  $\Delta E \sim 12 B_9$  eV, where  $B_9 = B/(10^9 \text{G})$  (Loeb 2003), so as long as  $B_9 < 1$  (as is usual in LMXB) then this is still narrow for the SXS.

However, there is also rotational broadening, with  $\Delta E \sim 1600(\nu_{spin}/600\text{Hz})(R/10\text{km})$  eV (Ozel 2013), and this is a clear issue as most LMXRB (i.e. systems with  $B < 10^9$  G as required) have spins  $\nu_{spin} = 185 - 650$  Hz (Pappitto et al. 2011).

Thus the only way to have any significant chance to recover narrow atomic features is to have an accreting NS where the surface is not too highly ionised (i.e. not strong X-ray bursts) and can be seen directly (i.e. not the high mass accretion rate upper banana branch or Z sources). More stringently, to see these features as narrow requires that the line of sight velocity component from the surface is small (slow spin NS, pole on faster spin

NS, phase resolved small spot on NS), and that the magnetic field is low.

Any target meeting these requirements should be a high priority PV observation.

## 2.3 Targets & Feasibility

### 2.3.1 Low inclination

Normal spin systems which are viewed at low inclination ( $< 30^\circ$ ) can still show a narrow core to the line profile, even though the majority of the line is rotationally broadened (Baubock, Psaltis & Ozel 2013). There is one atoll system, Ser X-1, where optical spectroscopy of the 2 hour binary orbit indicates a low inclination,  $i < 10^\circ$  (Cornelisse et al. 2013). A low inclination is also consistent with the non-detection of dips in the X-ray lightcurves (the structures in the MAXI long term light curves are not real: Shidatsu, private communication), and the lack of any burst oscillations in the X-ray burst lightcurves (Galloway et al. 2008). This persistent system is always in the soft state (mid banana branch,  $L/L_{Edd} \sim 0.3$  for 7.7 kpc), so the disk should extend down close to the NS surface, consistent with the iron line broadening seen by *NuSTAR* (Miller et al. 2013).

We fit the *Suzaku* XIS (black) and HXD (grey) data with a model incorporating the disk (diskbb: red), NS surface (bb: magenta), Comptonised boundary layer (nthcomp: blue) and its reflection (kdblur×rfxconv×nthcomp: cyan). This gives  $\chi^2_\nu = 1115/598$ . The observed blackbody temperature from the NS surface is  $\sim 0.6$  keV. This is gravitationally redshifted, so the intrinsic surface temperature is a factor  $1.2 - 1.3\times$  higher. This intrinsic photospheric emission is not a true blackbody, but can be approximated by a colour temperature corrected blackbody, where the colour temperature correction factor  $f_{col} \sim 1.4 - 1.5$  (Suleimanov et al. 2012). This cancels out most of the redshift, so the intrinsic photosphere temperature should be similar to the observed blackbody temperature at  $\sim 0.6$  keV. This is cool enough that there can easily be atomic features present.

We replace the blackbody in the fit with a NS photosphere model at 6M K (V. Suleimanov, private communication). We convolve this with the full transfer function expected from a NS rotating at 400 Hz (a typical spin) viewed at  $10^\circ$ , assuming a mass of  $1.4M_\odot$  and 10 km radius (M. Baubock, private communication), corresponding to  $\log g = 14.27$ . This is effectively the same as convolving the photosphere model with gsmooth with  $\Delta E = 0.05$  keV at 6 keV, and  $\Delta E/E = 1$ , together with a redshift  $z_{\text{surface}} = 0.305$ . This shows that there are 4 main absorption features at this temperature (see Fig 1a), FeXXV at  $1.8508\text{\AA}$ , a blend of ArXVII Ly $\alpha$  ( $3.9493\text{\AA}$ ) with SXVI Ly $\beta$  ( $3.9908\text{\AA}$ ) at mean wavelength of  $3.9700\text{\AA}$ , CaXIX at  $3.1773\text{\AA}$  and SXVI at  $4.7328\text{\AA}$ .

We fit the full photosphere/transfer function model to the *Suzaku* data, but allow the NS temperature to be slightly different than the tabulated model by multiplying the 6M K template by a further redshift ( $z_{\text{AShift}}=0.039$ ), showing that the data prefer a slightly lower intrinsic photosphere temperature. We get a slightly better fit for this more realistic photosphere model than with the pure blackbody, with  $\chi^2 = 997/597$  (one fewer degree of freedom as the seed photons for Comptonisation are no longer tied to the NS temperature) but this is due to the fact that the data prefer the broader continuum over a narrower blackbody, rather than *Suzaku* detecting the lines. The 4 main lines have equivalent width of 2.2eV (FeXXV), 1.8 eV (CaXIX), 1.8eV (ArXVII/SXVI) and 1.9eV (SXVI) against this continuum model.

We simulate this model, which includes the photospheric lines with total redshift  $z_{\text{surface}} = 1.305 \times 1.039 - 1 = 0.356$ , through the SXS, using the 7eV resolution response. This gives a count rate of  $\sim 350$  c/s so we use the neutral density filter to reduce this to 88 c/s. We resimulate this for 50 ks and 100 ks, and fit each dataset in the 1-10 keV bandpass with the original *Suzaku* model i.e. with a blackbody for the NS surface. The lines are clearly detected in all simulations by plotting the resulting  $\chi^2$ .

We then add in the 4 narrow gaussians, all with the same broadening (gsmooth with  $\Delta E = 0.05$  keV at 6 keV, and  $\Delta E/E = 1$ ) and redshift ( $z_{\text{AShift}}$ ). These are very significantly detected in both simulations, with  $\Delta\chi^2 = 136$  and 220 for 50 ks and 100 ks, respectively. Both return the input  $z_{\text{surface}} = 0.356$  both with uncertainties of  $\sim 1\%$  due to the width of the lines.

The significance of the detection is mainly due to the two low energy lines, as can clearly be seen in the  $\chi^2$  residual plot to the continuum models. In the 50 ks simulation,  $\Delta\chi^2$  for each line is 15 (Fe), 22 (Ca), 53 (Ar/S) and 47 (S). Thus this is clearly feasible to detect all 4 lines even in 50ks, but this did not allow for

pileup/PSP/telemetry limitations. To derive a similarly good spectrum in only high+medium resolution counts will probably take 100ks of observing time.

However, the most significant lines are at energies where it should also be possible for the *Chandra* gratings to detect them, though chip gaps mean the sensitivity is reduced at 1.95 and 2.3 keV. There are currently 150ks of *Chandra* METG/HETG data (soon to be increased by another 150ks). A preliminary analysis of these data (E. Cackett, private communication) shows no obvious features at this level. A more detailed analysis of the *Chandra* grating data should be able to constrain the line equivalent widths even if they are a factor 2 smaller than predicted here. An upper limit (as opposed to a marginal detection) from *Chandra* would imply the photosphere abundances of these elements at the poles is less than  $\approx 0.5 - 1 \times$  solar.

The models used here assumed solar abundances, as indicated from the strength of reflected iron line observed from the accretion disk. There is significant uncertainty on the abundance distribution over the NS surface both due to the spallation (Chang et al. 2005), and due to the spatial inhomogeneity of the accretion flow. Accretion is expected to occur in an equatorial belt, so a pole-on view gives an unobscured view of the NS surface, but could be dominated by material where the heavy elements have settled out and are not replenished by accretion. This source has X-ray bursts (Galloway et al. 2008, 0.1 per hour so expect 2-3 in 100 ks, though there appear to be none in the 150ks *Chandra* data) which should dredge up the elements over the whole surface, but these can sink rapidly after the burst (see e.g. Özel 2013). A 100ks *ASTRO-H* observation would tightly constrain the elemental composition of the NS crust at the poles.

The cool phase of the bursts can additionally be searched for atomic features since the abundances here may be extremely supersolar due to dredge up.

### 2.3.2 Beyond Feasibility: low inclination

All the burst spectra can give 10-20% constraints on  $M/R$  from the measured luminosity and temperature of the burst.

The HXI and SGD together will trace the shape of the continuum at high energies. The *Swift* BAT already shows that there is no persistent hard tail which extends out to higher energies, but the *Suzaku* HXD and *NuSTAR* data show that the shape of the rollover is not completely matched by a single temperature Comptonised spectrum and its reflection. Simultaneous data at high energies will show whether the Comptonised boundary layer has some range in temperature, as predicted by models of the spreading equatorial belt (Suleimanov & Poutanen 2006).

The reflection spectrum from the accretion disk again can give 10-20% constraints on  $M/R$  from the iron line profile (e.g. Miller et al. 2013).

### 2.3.3 Slow spin

The slowest known NS spin system is IGR J17480-2446 in Terzan 5 (T5X2 hereafter) where  $\nu_{spin} = 11$  Hz, equivalent to 30 eV in rotational broadening. However, this is also an AMXP, with inferred magnetic field of few  $\times 10^8 - 10^{10}$  G (Miller et al. 2011; Cavecchi et al. 2011; Patruno & Watts 2012). Zeeman broadening dominates over rotational broadening at the upper end of this range, with predicted width of 100 eV, but the detected high frequency QPO in this system constrains the field to the lower range (Barret 2012).

The next slowest spin system is the accreting millisecond pulsar XTE J0929-314 at 185 Hz (the 45 Hz claimed spin from EXO0748 is now known to be spurious with the true spin at 550 Hz, and the 95 Hz signal from XB 1254-690 is only a  $2\sigma$  detection see e.g. the compilations in Patruno & Watts 2012; Özel 2013). Hence rotational broadening is over 300 eV, making the features undetectable. Thus currently the only known slow spin system is T5X2.

As this is an AMXP the accretion geometry can be rather different to that of the standard LMXB. At low mass accretion rates, the quasi-spherical hot accretion flow can be collimated by the B field, forming a shock when it hits the NS surface. Hard X-ray emission from the shock illuminates the NS surface close to the magnetic pole, forming a hotspot. Evidence for this is seen from the different pulse profiles of the (blackbody) hotspot and hard X-ray Comptonised emission from the shock (e.g. Gierlinski, Done & Barret 2002). Hence it is clear

in this state that we do see part of the NS surface directly. There should also be a cooler component from the unilluminated NS surface further from the shock, and an even cooler component from the truncated thin disk (e.g. Kajava et al. 2011).

T5X2 is also the only known AMXP to go to high enough mass accretion rates to go into the soft state. Here the disk should extend down (close to) the NS surface, and the pulsed fraction drops abruptly (though it is still detectable: Papitto et al. 2012). In fact, this source goes to such high luminosities that it becomes a Z source (Altamirano et al. 2010). There is a *Chandra* grating observation 5 days after the Z source peak, when the source had already dimmed down to the banana branch ( $L/L_{\text{Edd}} \sim 0.3$  for 5.9 kpc: Papitto et al. 2012; Chakraborty et al. 2011). The continuum spectrum is very similar to that from Ser X-1, and again there are no features from the NS surface in the *Chandra* data (Miller et al. 2011), though here the NS surface may be less visible than in Ser X-1 as T5X2 is not pole on. Thus for this source there is more chance of detecting the surface in an island state rather than on the banana branch.

T5X2 is a transient, and is currently in quiescence so we need to wait for another outburst. Figure 4a shows a model for a bright island state of SAX J1808.4-3658 (hereafter J1808) from Kajava et al. (2011), where the total (black) includes the disk (red), neutron star surface (green) and comptonised emission (blue). The grey line shows the NS surface from a 6M K solar abundance thermal NS model (V. Suleimanov, private communication), with surface redshift of 0.3. This is broader than than the blackbody, but this roughly matches the peak energy and normalisation component seen in the data.

We convolve the NS surface model with *gsmooth* with  $\Delta E/E = 1$  and an intrinsic line width of 30 eV at 6 keV as appropriate for the low spin of T5X2. We scale the entire model for the factor of 2 difference in distance between J1808 and T5X2, and replace the J1808 column of  $0.11 \times 10^{22} \text{ cm}^{-2}$  with  $1.5 \times 10^{22} \text{ cm}^{-2}$  for T5X2 (Miller et al. 2012). We simulate this model, including the full NS surface features, through the SXS response for 100ks. The count rate is 12 c/s so it is not piled up.

We fit the simulated SXS data (Fig4b) with a disk, blackbody and comptonisation model (red, green and blue lines, respectively), and there are clear residuals as shown in Fig 4c. As in the low inclination system Ser X-1 above, the largest features seen correspond to the same 4 lines, SXVI at 4.7328Å, a blend of ArXVII/SXVI at mean wavelength of 3.9700Å, CaXIX at 3.1773Å and FeXXV at 1.8508Å. We fit four negative gaussians at these energies, with redshift and broadening tied between them. While the SXVI line is the most significant (Fig 4c), it has EW of only 5 eV. The FeXXV line by contrast has an EW of 10 eV but the detector is less sensitive at energies of  $\sim 5 \text{ keV}$  than at  $\sim 2 \text{ keV}$ . The fit statistic decreases by  $\chi^2 = 350$  for the addition of the four lines so the derived redshift is well constrained at  $z_{\text{surface}} = 0.3 \pm 0.003$  and is unambiguous as it uses all 4 lines rather than relying on the identification of a single feature. The presence of other, weaker features means that the broadening is slightly overestimated, at  $65 \pm 10 \text{ eV}$  at 6 keV.

There is a drop in the effective area of the SXS feature in the response matrix at 2.18-2.3 keV. Sharp features in the response can cause narrow residuals if the energy scale is not properly calibrated. However, the edge in the current detector response is not particularly sharp, so is unlikely to cause confusion with a narrow line.

### 2.3.4 Beyond Feasibility: slow spin

Long observations in the island state are almost certain to sample X-ray bursts, with an average of 10 expected per 100ks observation (Galloway et al. 2008). There is the possibility that there are photospheric features in the burst spectra, especially at the coolest temperatures seen which are  $< 1.5 \text{ keV}$  where iron should not be completely ionised. Bursts from T5X2 give the possibility of seeing these features (Blidstein, Chang & Paerels 2003; Rauch, Suleimanov & Werner 2008). The burst continuum luminosity and temperature will also give constraints on M/R.

The T5X2 island state data show a low frequency (LF) QPO, which already challenges the Lense-Thirring model for this feature as the very slow spin in this system means that any torque between the spin and a misaligned accretion flow is small (Altamirano et al. 2013). Nonetheless, the LF QPO signal can still be split up as a function of QPO phase to search for the ‘smoking gun’ signature of precession of a vertically tilted flow, where the iron line profile shifts bluer before the phase of peak intensity of the QPO, and redder afterwards

(Ingram & Done 2012; see the *ASTRO-H* Black Holes white paper: Miller et al. 2014).

Island states should also show reflection from the accretion disk. The width of the broad line and the solid angle of the reflecting material together can show whether or not the inner thin disk is replaced by a hot flow as proposed in the truncated disk models. This can be constrained by spectral fitting alone, but the continuum is complex, with contributions from the disk, NS photosphere and Comptonisation spectrum as well as the reflected emission from the disk and perhaps some component of reflection from the NS surface (e.g. compare Cackett et al. 2010 and Egron et al. 2012; see also Sanna et al. 2013). However, the iron line and reflected continuum should also be lagged on a light crossing time, so a combination of spectral-timing techniques (which are currently being developed) may give better constraints.

### 2.3.5 Phase resolved emission

The accreting millisecond pulsars have pulsed emission showing that the accretion flow is collimated onto the magnetic pole. Phase resolved emission then limits the velocity broadening in each phase bin. For a small shock this could recover a narrow feature which shifted systematically with phase, but recent results indicate that this shock region is probably fairly extended in azimuth (Kajava et al. 2011), so atomic features will still be broadened by the velocity range from the NS surface even in a phase resolved analysis, making this unfeasible. All these systems are transients, so this would additionally require a ToO

## 3 Linking outflows to inflows in strong gravity: Winds in absorption

### 3.1 Background and Previous Studies

The radius of the NS is similar to that of the last stable orbit, so the gravitational potential seen by the accretion flow is the same as that of black holes (BH). Thus the accretion flow structures (disk, corona, disk jet, diskwinds) should be similar in both the NS and BH systems, though the presence of a surface in the NS gives an additional boundary layer continuum component, while an ergosphere could (but probably doesn't: Migliari & Fender 2006) give an additional spin powered jet in the BH.

Absorption lines from ionised material are seen in many LMXB systems, both NS and BH. These are most obvious during the deep absorption dips connected to the accretion stream impact on the disk which modulate high inclination sources on the orbital period, but there is also more highly ionised material seen mostly via iron  $K\alpha$  absorption lines present outside of the dips, showing that it is distributed above the disk at all azimuths (see e.g. the review by Diaz Trigo & Boirin 2012 for NS and Ponti et al. 2012 for BH). Key questions which can be addressed with the SXS on *ASTRO-H* are a) How is this material fed from the disk ? b) How much mass is lost in the wind and what is the impact of this on the accretion disk/jet structure ? c) Are there any differences between the winds in BH and NS systems ?

Again, the SXS on *ASTRO-H* has enormous discovery space in terms of the properties of this highly ionised material due to its factor of 10 better energy resolution at iron K, as well as a factor 10 increased effective area for sources below  $\sim 4 \times 10^{-9}$  ergs cm $^{-2}$  s $^{-1}$  (pileup count rate limitations cut in above this flux).

### 3.2 Prospects & Strategy

X-ray irradiation of the disk must produce a thermally driven wind/corona. The X-ray flux from the innermost regions illuminates the upper layers of the outer disk, heating it up to the Compton temperature,  $T_{IC}$  (which depends only on spectral shape). The heated upper layer expands on the sound speed  $v_{IC} = (kT_{IC}/(\mu m_p))^{1/2}$  due to the pressure gradient, so the thermal energy driving the expansion is larger than the binding energy at radius  $R_{IC} = (1 - L/L_{Edd})(v_{IC}/c)^{-2} R_g = 6 \times 10^5 (1 - L/L_{Edd})(kT_{ic}/10^7 \text{ K})^{-1} R_g = 10^{12} (1 - L/L_{Edd})(kT_{ic}/10^7 \text{ K})^{-1} (M/10M_\odot) \text{ cm}$  so the material escapes as a wind (Begelman et al. 1983). A more careful treatment shows that this leads to a wind from the outer disk when  $R > 0.2R_{IC}$  and the luminosity is bright enough to sustain rapid heating. Conversely, at smaller radii/lower luminosity the material remains bound but

forms an extended atmosphere above the disk (Begelman et al. 1983, Woods et al. 1996; Jimenez-Garate et al. 2002).

The strong X-ray illumination from the central source/inner accretion disk ionises the wind, and the ionisation parameter  $\xi = L/nR^2$  can be estimated from the ratio of H to He-like absorption line equivalent width (EW). However, these EW's are set by a combination of the column density in that ion species, together with the turbulent velocity in the wind. CCD resolution only gives an upper limit for the velocity width of the line, which typically can be produced from a wide range of column densities (saturated regime of the curve of growth). This uncertainty on column combines with uncertainty from the geometry ( $N_H = n\Delta R < nR$ ) in estimating the launch radius  $R < L/(\xi N_H)$ .

Current data from the NS systems show a good match to the thermal wind predictions, as the absorbing material with inferred small radii is static, while outflows are only seen at radii larger than  $0.2R_{IC}$  (Diaz Trigo & Boirin 2012). This is in contrast to the controversy over the wind driving mechanism in black hole LMXB systems. Many winds in the black hole systems are also consistent with thermal driving, but the dramatic absorption seen in one observation of GRO J1655-40 requires additional mass loss, probably indicating magnetic driving (Miller et al. 2006; Luketic et al. 2010) unless the wind is so thick as to cause the source luminosity to be severely underestimated (Done, Gierlinski & Kubota 2007). The fact that such extreme winds are not seen from *any* of the short period (small disk, persistent) high inclination (dipping) NS systems (Diaz Trigo & Boirin 2012) strongly argues against any similar magnetic driving being important in the NS. A single observation of Cir X-1 is the only counterexample of an NS wind outside of the thermal wind region (Diaz Trigo & Boirin 2012), but the spectral complexity often seen from this source means that its luminosity could be strongly underestimated.

*ASTRO-H* will improve on this by giving a direct measure of the turbulent velocity, to give a well constrained ion column from the observed equivalent width. The improved sensitivity at high energy coupled with the better energy resolution means that it is likely that the weak  $K\beta$  absorption lines will be independently detected and constrained. These are not saturated so they give an unambiguous measure of the ion column density.

The mass loss due to a thermal wind increases with increasing disk radius (Begelman et al. 1983; Woods et al. 1996), hence for the longest period systems the prediction is that the mass loss rate is a factor few larger than the observed mass accretion rate onto the compact object. This mass loss rate can be measured from the ratio of emission to absorption (P Cygni profile) seen in the wind lines. The best current data from *Chandra* currently only give an upper limit to the solid angle subtended by the wind as less than a third of that expected from a spherical wind in GX13+1 (Ueda et al. 2004). The much better resolution of the SXS should enable a detection of the associated emission, and hence give a direct measure of the mass loss rate in the wind.

In thermal wind models, the intrinsic line width is set mostly by the velocity profile (decreasing with launch radius along the disk but increasing with height as the material is accelerated by the thermal expansion) rather than by true turbulence. The high resolution line profiles of unsaturated lines should constrain this, allowing the acceleration law to be reconstructed. The profiles should also constrain the solid angle of the wind through the ratio of emission to absorption, allowing the total mass loss rate to be determined. All these features (launch radius, outflow velocity, velocity profile, mass loss rate) can then be critically compared to the thermal wind models to stringently test these against the first data which can properly resolve the velocity structure.

### 3.3 Targets & Feasibility

Many NS systems are physically small, so their disks do not extend far enough to power a wind, so they can only show static coronae. However, systems with evolved companions have larger orbits and hence larger disks, so are more likely to show wind features. However, large disks are also more likely to trigger the Hydrogen ionisation instability, so these systems are transient unless the mass transfer rate from the companion is very high (King & Kolb 1999). Data from the NS systems show that the ionised material is significantly blueshifted (i.e. is a wind) only where its inferred distance is larger than  $0.2R_{IC}$  (GX13+1, with very long orbital period of  $\sim 24$  days, and the transient T5X2), and that the outflow velocity is of order the escape velocity at the launch radius, so  $v_{IC} = (R/R_g)^{-1/2}c \sim 500 - 3000 \text{ km s}^{-1}$  for  $0.2R_{IC}$ , consistent with a thermal wind.



The LMXB catalog of Liu et al. (2007) shows that GX13+1 is the only long period sub-Eddington (atoll rather than Z source) system. It is persistent, so scheduling is not an issue, and it persistently shows absorption lines from Fe XXV and XXVI (Ueda et al. 2001; 2004; Diaz Trigo et al. 2012), as well as lower equivalent width features from Hydrogen-like Mn, Cr, Ca, Ar, S, Si, and Mg. The lines have a blueshift of  $\sim 450 \text{ km s}^{-1}$  and an intrinsic width of  $\sim 490 \pm 110 \text{ km s}^{-1}$  (i.e. at the limit of the *Chandra* HETG resolution). The lines will be easily resolved with the SXS. Fig 5a shows a simulation of a 50 ks SXS spectrum, with flux reduced by a factor 3 to give a countrate of 65 c/s. The model `tbabs×zxipcf×(diskbb+body+gau)` has an ionised absorber with column of  $3 \times 10^{23} \text{ cm}^{-2}$  and  $\log \xi = 4.41$  (similar to that seen by Ueda et al. 2004). Fig 5b shows a close up of the resolved line profile around Fe XXVI  $K\alpha$ . This ionised absorber was simulated with a turbulent velocity of 200 km/s and is easily resolved by the SXS, and is clearly saturated, being completely black in the center. None of the other lines are saturated, so the column can be measured unambiguously from the Fe XXVI  $K\beta$  line.

However, winds are not dominated by turbulent velocities. Instead, their velocity structure is determined by the acceleration mechanism, imprinting itself onto the (unsaturated) line profiles. Standard P-Cygni lines can be fit assuming a simple model for the column at each velocity of  $\tau(v) \propto (1 - v/v_\infty)^\alpha$ . The red and black lines in Fig 5c show what happens to the line shapes for different acceleration laws, parameterised by different  $\alpha$  and  $v_\infty$ . Thermals winds have the majority of the acceleration happen close to the launch radius, so most of the material is outflowing at the terminal velocity (red line:  $\alpha = 0.2$  with  $v_\infty = 450 \text{ km/s}$ ). By contrast, magnetic driving could give rise to much slower acceleration, where the majority of the absorption occurs for material which is not yet at its terminal velocity (black line:  $\alpha = 4$  with  $v_\infty = 900 \text{ km/s}$  scaled to the same depth). The change in shape of the blue wing of the absorption line can be seen in a 100 ks *ASTRO-H* simulation (red and black points) of a source with 2-10 keV count rate of 45 counts/s in the SXS, though it may be possible to recover this significance from a 50 ks observation by stacking the line profiles from all unsaturated lines. These different velocity structures give the most sensitive diagnostic of the launch mechanism.

The models in Fig 5c were for a pure P-Cygni profile (Lamers et al. 1987; Done et al. 2007) i.e. assuming a spherically symmetric winds, so give maximum emission associated with the absorption. The *Chandra* HETG already limits the solid angle of the wind to be less than a third of this maximum (Ueda et al. 2004), so the emission in these profiles is overestimated. Fitting the detailed line profiles should determine the ratio of emission to absorption, and hence give an unambiguous measure of the solid angle of the wind as required to determine the total mass loss rate. More theoretical work to develop P-Cygni profiles from diskwinds should be done so that these models can explicitly be fit to the data to constrain the solid angle of the wind.

### 3.4 Beyond Feasibility

GX13+1 is in the upper banana branch, so should have its disk be close to the NS surface. The broad iron line is clearly seen in the *XMM-Newton* datasets (Diaz-Trigo et al. 2012). The width of the line should determine the inner radius of the disk, and hence give an upper limit to the size of the NS surface.

This source also shows weak evidence for a hard tail above 50 keV from *INTEGRAL* data (Paizis et al. 2006). The HXT and SGD will be able to constrain this component with much greater confidence, so that its nature and origin can be better understood.

## 4 Linking outflows to inflows in strong gravity: Winds in emission

### 4.1 Background and Previous Studies

LMXB seen at very high inclination have the inner disk completely obscured by the outer disk so the source is seen only indirectly through scattering in the corona and wind, though this reflected emission is also overlaid by recombination from the photoionised corona and wind. These are called accretion disk corona (ADC) sources, and they give a different angle on the corona and wind structure above the disk than seen in the absorption lines discussed above.

## 4.2 Prospects & Strategy

The spectrum of emission lines from the X-ray heated wind and/or corona above the disk is extremely rich in plasma diagnostics (e.g. the theoretical calculations of the corona by Jimenez-Garate et al. 2002 shown in Fig 6).

## 4.3 Targets & Feasibility

To compare the wind features (not just the static corona) requires that we use an ADC which has a large enough orbital period to drive a wind. This uniquely selects 2S0921-63, the longest period ADC source (9.02 days e.g. Kallman et al. 2003). This shows true eclipses as well as orbital ADC modulation, and the eclipse gives the cleanest possible diagnostic of the scattering material at large distances from the source, weighting the emission to the wind region rather than the static corona below  $0.2R_{IC}$ . The eclipse lasts up to 80 ks, setting the upper limit to the time for a single observation, with 2-10 keV flux of  $9 \times 10^{-11}$  ergs cm<sup>-2</sup> s<sup>-1</sup> (EPIC PN) with strong line emission from Fe XXV and XXVI as well as multiple species at lower energy (Kallman et al. 2003). The iron  $K\alpha$  (and  $\beta$ ) line intrinsic widths should uniquely determine the wind outflow velocity. These emission lines should also be accompanied by absorption lines, though these are much reduced due to the geometry. These intrinsic line widths are not well constrained by the EPIC PN and MOS cameras due to their poor resolution, with width  $< 1300$  km/s, nor are they well constrained by the *Chandra* HETG data due to low statistics.

We simulate an 80 ks eclipse spectrum using the *XMM-Newton* data reported in Kallman et al. (2003) giving 4 cts/s in the SXS (Fig 7). The Fe  $K\alpha$  lines are simulated assuming these are from a wind with outflow velocity of 450 km/s, giving an intrinsic width of 450 km/s (i.e. 0.01 keV). This intrinsic width of both 6.7 and 6.95 keV emission lines can be easily constrained in the 80 ks simulation, showing that this is detecting emission from the wind.

The alternative bright ADC source X1822-371 has much shorter orbital period of 5.57 hours. This gives an implied disk size of  $\sim 5 \times 10^{10}$  cm, which is just large enough for a thermal wind to form, especially as this system is probably intrinsically close to  $L_{Edd}$ . There are existing *Chandra* HETG spectra of this source which show a weak FeXXVI resonance line which is consistent with coming from the static corona/outflow region with  $R < 3.7 \times 10^{10}$  cm (from eclipse location). This emission line is narrow, with  $\sigma < 400$  km/s (Ji et al. 2011; Iaria et al. 2013), implying that the wind outflow velocity is of this order. This seems surprisingly small for a system close to  $L_{Edd}$ . Most of the other lower ionisation lines come from material associated with the disk edge (Ji et al. 2011; Iaria et al. 2013).

## 4.4 Beyond Feasibility

Bursts are unlikely to be seen as the source is intrinsically quite luminous, so should be in the regime of stable nuclear burning. However, the lower energy line emission spectrum should be extremely rich, allowing multiple other diagnostics of the wind and corona.

# 5 Spectral modelling requirements

There is still much work to be done on model development in order to access the full science from SXS observations. These are:

Section 1 on the NS equation of state. The models of the NS surface spectra have so far only been calculated for purely thermal emission. However, the island state has a strong hard X-ray component which will illuminate the surface, potentially changing the gradient in ionisation state with scale height. These effects should be incorporated into the models in order to get a better estimate of the predicted equivalent width of the absorption lines. However, any significant detection of these absorption lines is a clean measure of  $M/R$  so this is not required to interpret the data if the lines are seen. More fundamentally, models of the abundance of the NS surface during steady accretion (rather than bursts) are highly uncertain, and it is possible that the heavy elements do sink below the photosphere so that there are no atomic features from the surface at all.

Section 2 on the wind in absorption from LMXRB. The wind absorption will likely be first characterised using the XSTAR photoionisation absorption models. These have recently been extended to include the doublet structure of the  $K\alpha$  line from H-like iron, however the data will also require this for He-like iron as well.

The emission associated with the wind cannot be calculated just using the (spherical) P Cygni approach as the wind is equatorial. Better models which include the emission and absorption for a given geometry are needed to get the tightest constraints from the observed line profiles. Updated (Woods et al. 1996) hydrodynamic simulations of thermal winds including radiation transfer are needed to make detailed predictions of the absorption line profiles predicted by thermal wind models.

Section 3 on the wind in emission from ADC LMXRB. There are sophisticated models, but there needs to be a lot of development to bridge between the models and diagnostics of the wind versus static corona and the dipping material.

## 6 Summary of Top Science

1. **Objective:** Measure  $M/R$  of a NS to a few percent.

**Why:** To constrain the equation of state of dense matter to order of magnitude better accuracy than the 10-20% from current measurements.

**How:** By detecting absorption lines from the surface of a neutron star with low projected velocity from rotation. This requires either low inclination (the steady source Ser X-1, on the banana branch where the NS surface at the poles should be seen directly) or slow rotation (the transient source T5X2, an 11 Hz AMXP, where the surface should be directly visible in the island state, requiring a ToO).

2. **Objective:** To measure the velocity profile of the accretion disk wind

**Why:** To determine how the wind is launched and accelerated.

**How:** Thermal wind models make some very specific predictions about the radial structure of the wind - its launch radius and its velocity profile. These are testable from high signal-to-noise SXS observations of the H and He-like absorption (and emission) lines in both  $K\alpha$  and  $\beta$ .

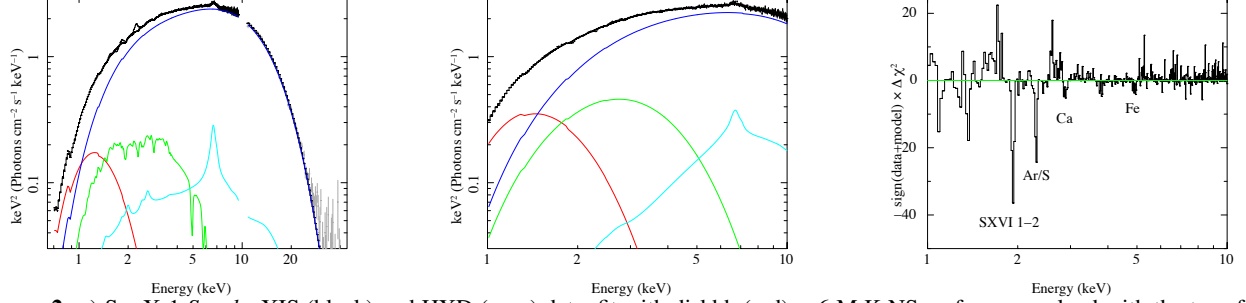


**Figure 2:** a) Ser X-1 *Suzaku* XIS (black) and HXD (grey) data, fit with diskbb (red) + 6 M K NS surface convolved with the transfer function expected for  $10^\circ$  inclination (green) + Comptonised boundary layer with seed photons at  $\sim 6$  M K (blue) and its reflection (cyan). b) The spectrum in a) simulated through the SXS with the neutral density filter for 50 ks. The model is as in a) except that the NS surface is replaced by a blackbody (green). c) residuals from the data/model fit in b) clearly showing the 4 main absorption lines seen in the model in a).

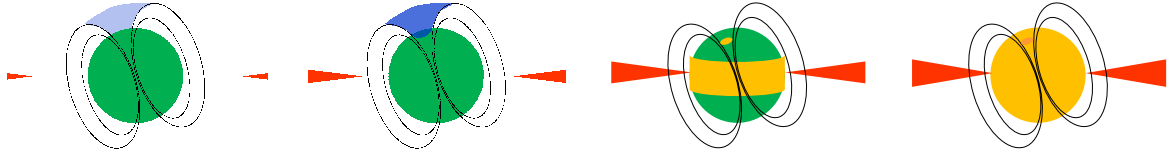


**Figure 3:** As in Figure 1 but for the AMXP where the magnetic field (black) is dynamically important and can collimate part of the accretion flow onto the magnetic poles.

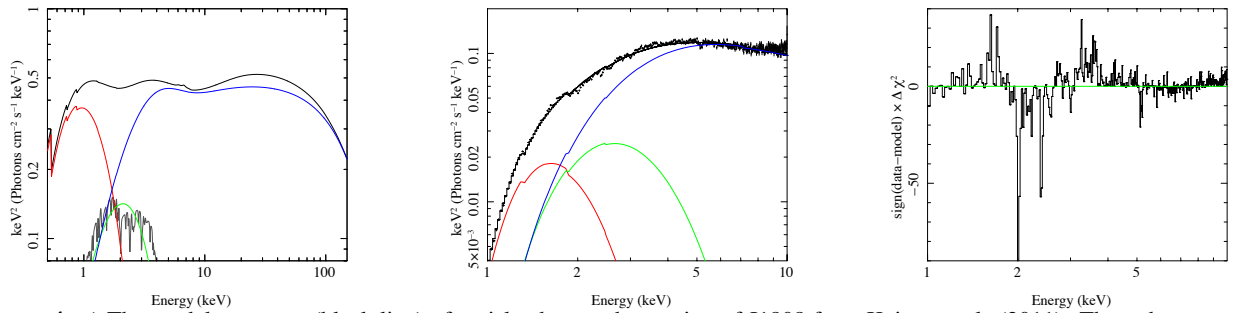


**Figure 4:** a) The model spectrum (black line) of an island state observation of J1808 from Kajava et al. (2011). The red, green and blue lines show the accretion disk, NS surface and corona, respectively. The grey line shows an NS surface photosphere model, scaled to best match the inferred surface emission in J1808. b) The model from a) including the NS photosphere, scaled to the distance of T5X2 and with  $N_H = 1.5 \times 10^{22} \text{ cm}^{-2}$  simulated through the SXS response for 100ks. This is fit with a continuum model with a disc (red) and corona (blue) but the NS surface is assumed to be a blackbody (green), i.e. without spectral features. c) Residuals to the fit in b), showing the absorption lines from SXVI ( $\sim 2$  keV), ArXVII/SXVI blend, CaXIX and FeXXV ( $\sim 5$  keV). Together these give an unambiguous, accurate measurement of  $M/R$ .

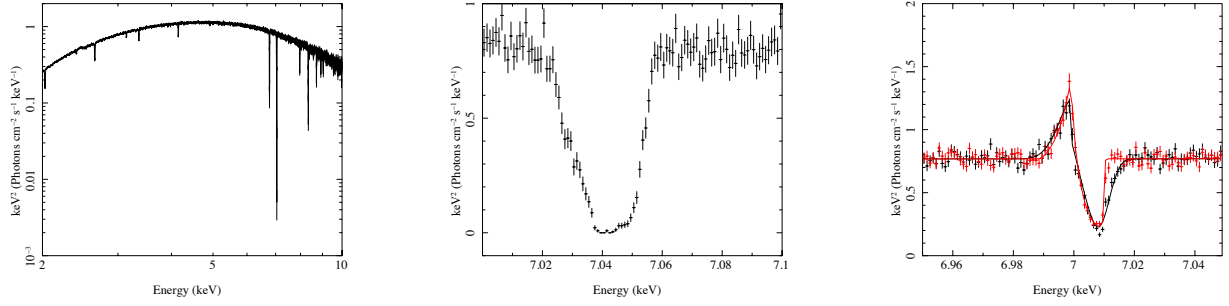


**Figure 5:** a) The overall spectrum of GX13+1 simulated for 50 ks, similar to that seen with the *Chandra* HETG (Ueda et al. 2004). Multiple absorption lines are easily seen. b) Close up of the strongest Fe line from (a), showing that it is saturated. c) Red line: absorption/emission line P Cygni profile from a wind which accelerates quickly, so most material is at the terminal velocity, as expected for thermal winds. The black line is normalised to the same line shift and equivalent width, but has a much slower acceleration profile. The difference in the blue wing of the absorption is significantly detected.

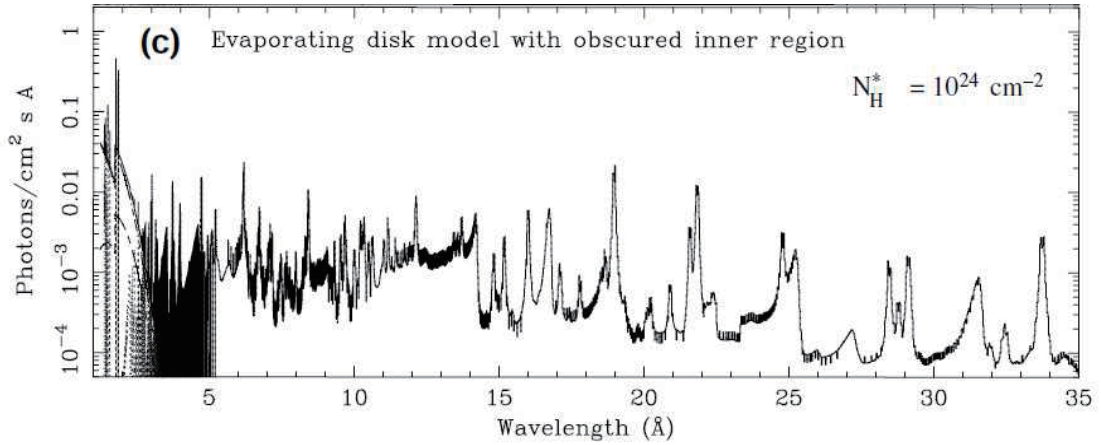


**Figure 6:** The recombination line and continuum spectrum from a corona above a NS disk where the central NS and disk is obscured by a column of 10<sup>24</sup> cm<sup>-2</sup> (Jimenez-Garate et al. 2002)

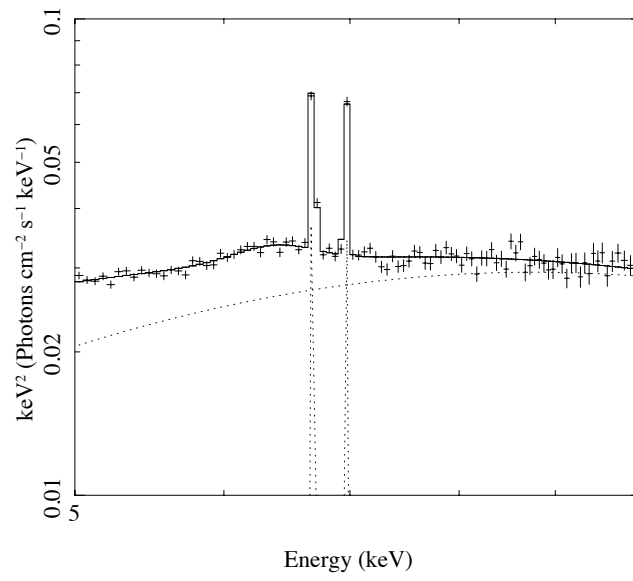


**Figure 7:** Simulated 80 ks eclipse spectrum of 2S0921-63. The data can easily determine the intrinsic width of the Fe XXV and XXVI emission lines, and hence constrain the velocity of the scattering material.

## References

- Altamirano, D., Watts, A., Kalamkar, M., et al. 2010, The Astronomer’s Telegram, 2932, 1
- Altamirano, D., Homan, J., Linares, M., et al. 2010, The Astronomer’s Telegram, 2952, 1
- Altamirano, D., Ingram, A., van der Klis, M., et al. 2012, ApJ.Letts., 759, L20
- Barret, D. 2012, ApJ., 753, 84
- Bauböck, M., Psaltis, D., Ozel, F. 2013, ApJ, 766, 87
- Begelman, M. C., McKee, C. F., & Shields, G. A. 1983, ApJ., 271, 70
- Bildsten, L., Chang, P., & Paerels, F. 2003, ApJ.Letts, 591, L29
- Cackett, E. M., Miller, J. M., Ballantyne, D. R., et al. 2010, ApJ, 720, 205
- Cavecchi, Y., Patruno, A., Haskell, B., et al. 2011, ApJL, 740, L8
- Chakraborty, M., Bhattacharyya, S., & Mukherjee, A. 2011, MNRAS, 418, 490
- Chang, P., Bildsten, L., & Wasserman, I. 2005, ApJ., 629, 998
- Cornelisse, R., Casares, J., Charles, P. A., & Steeghs, D. 2013, MNRAS, 432, 1361
- Cumming, A., Zweibel, E., & Bildsten, L. 2001, ApJ, 557, 958
- Diaz Trigo, M., & Boirin, L. 2012, arXiv:1210.0318
- Díaz Trigo, M., Sidoli, L., Boirin, L., & Parmar, A. N. 2012, A&A, 543, A50
- Done, C., Gierliński, M., & Kubota, A. 2007, ARA&A, 15, 1
- Done, C., Sobolewska, M. A., Gierliński, M., & Schurch, N. J. 2007, MNRAS, 374, L15
- Egron, E., Di Salvo, T., Motta, S., et al. 2013, A&A, 550, A5
- Frank, J., King, A., & Raine, D. J. 2002, Accretion Power in Astrophysics, by Juhan Frank and Andrew King and Derek Raine, pp. 398. ISBN 0521620538. Cambridge, UK: Cambridge University Press, February 2002.
- Galloway, D. K., Munro, M. P., Hartman, J. M., Psaltis, D., & Chakrabarty, D. 2008, ApJ.Supp., 179, 360
- Gierliński, M., Done, C., & Barret, D. 2002, MNRAS, 331, 141
- Hebeler, K., Lattimer, J. M., Pethick, C. J., & Schwenk, A. 2013, ApJ, 773, 11
- Iaria, R., Di Salvo, T., D’Aì, A., et al. 2013, A&A, 549, A33
- Ingram, A., & Done, C. 2012, MNRAS, 427, 934
- Ji, L., Schulz, N. S., Nowak, M. A., & Canizares, C. R. 2011, ApJ., 729, 102
- Jimenez-Garate, M. A., Raymond, J. C., & Liedahl, D. A. 2002, ApJ., 581, 1297
- Kallman, T. R., Angelini, L., Boroson, B., & Cottam, J. 2003, ApJ., 583, 861
- Kajava, J. J. E., Ibragimov, A., Annala, M., Patruno, A., & Poutanen, J. 2011, MNRAS, 417, 1454
- King, A. R., Kolb, U., & Burderi, L. 1996, ApJL, 464, L127
- King, A. R., & Kolb, U. 1999, MNRAS, 305, 654
- Lamb, F. K., Boutloukos, S., Van Wassenhove, S., et al. 2009, ApJ, 706, 417
- Lamers, H. J. G. L. M., Cerruti-Sola, M., & Perinotto, M. 1987, ApJ, 314, 726
- Lin, D., Remillard, R. A., & Homan, J. 2009, ApJ., 696, 1257
- Loeb, A. 2003, Physical Review Letters, 91, 071103
- Liu, Q. Z., van Paradijs, J., & van den Heuvel, E. P. J. 2007, A&A, 469, 807
- Luketic, S., Proga, D., Kallman, T. R., Raymond, J. C., & Miller, J. M. 2010, ApJ., 719, 515
- Medvedev, M. V., & Narayan, R. 2001, ApJ, 554, 1255
- Migliari, S., & Fender, R. P. 2006, MNRAS, 366, 79
- Miller, J. M., Raymond, J., Fabian, A., et al. 2006, Nature, 441, 953
- Miller, J. M., Maitra, D., Cackett, E. M., Bhattacharyya, S., & Strohmayer, T. E. 2011, ApJL, 731, L7
- Miller, J. M., Parker, M. L., Fuerst, F., et al. 2013, ApJL, 779, L2
- Özel, F. 2013, Reports on Progress in Physics, 76, 016901
- Papitto, A., Di Salvo, T., Burderi, L., et al. 2012, MNRAS, 423, 1178
- Papitto, A., Ferrigno, C., Bozzo, E., et al. 2013, Nature, 501, 517
- Patruno, A., & Watts, A. L. 2012, arXiv:1206.2727
- Paizis, A., Farinelli, R., Titarchuk, L., et al. 2006, A&A, 459, 187
- Ponti, G., Fender, R. P., Begelman, M. C., et al. 2012, MNRAS, 422, L11
- Rauch, T., Suleimanov, V., & Werner, K. 2008, A&A, 490, 1127
- Revnivtsev, M. G., Suleimanov, V. F., & Poutanen, J. 2013, MNRAS, 434, 2355
- Sakurai, S., Torii, S., Noda, H., et al. 2014, PASJ, 66, 10
- Sanna, A., Hiemstra, B., Méndez, M., et al. 2013, MNRAS, 432, 1144
- Suleimanov, V., & Poutanen, J. 2006, MNRAS, 369, 2036
- Suleimanov, V., Poutanen, J., & Werner, K. 2012, A&A, 545, A120
- Ueda, Y., Asai, K., Yamaoka, K., Dotani, T., & Inoue, H. 2001, ApJ.Letts, 556, L87
- Ueda, Y., Murakami, H., Yamaoka, K., Dotani, T., & Ebisawa, K. 2004, ApJ., 609, 325
- Woods, D. T., Klein, R. I., Castor, J. I., McKee, C. F., & Bell, J. B. 1996, ApJ., 461, 767